INDUCER HYDRODYNAMIC LOAD MEASUREMENT DEVICES

Stephen E. Skelley and Thomas F. Zoladz
George C. Marshall Space Flight Center
Marshall Space Flight Center, AL 35812

ABSTRACT

Marshall Space Flight Center (MSFC) has demonstrated two measurement devices for sensing and resolving the hydrodynamic loads on fluid machinery. The first — a derivative of the six-component wind tunnel balance — senses the forces and moments on the rotating device through a weakened shaft section instrumented with a series of strain gauges. This rotating balance was designed to directly measure the steady and unsteady hydrodynamic loads on an inducer, thereby defining both the amplitude and frequency content associated with operating in various cavitation modes. The second device — a high frequency response pressure transducer surface mounted on a rotating component - was merely an extension of existing technology for application in water. MSFC has recently completed experimental evaluations of both the rotating balance and surface-mount transducers in a water test loop. The measurement bandwidth of the rotating balance was severely limited by the relative flexibility of the device itself, resulting in an unexpectedly low structural bending mode and invalidating the higher-frequency response data. Despite these limitations, measurements confirmed that the integrated loads on the four-bladed inducer respond to both cavitation intensity and cavitation phenomena. Likewise, the surface-mount pressure transducers were subjected to a range of temperatures and flow conditions in a non-rotating environment to record bias shifts and transfer functions between the transducers and a reference device. The pressure transducer static performance was within manufacturer's specifications and dynamic response accurately followed that of the reference.

INTRODUCTION

The experimental tests were proposed in response to recent experiences with turbomachinery cavitation, especially in systems using liquid oxygen, and the potentially catastrophic effects of this hydrodynamic phenomenon. High-performance rocket engine systems by design operate near the limits of structural integrity and often encounter unexpected phenomena, which, in turn, may trigger unexpected system responses such as excessive vibration, rotating and stationary component contact, or elevated bearing loads. Any or all of these system responses may stem from a relatively small area of intense cavitation, and are often amplified by system structural modes or rotordynamic performance. An example of system response to pump cavitation includes the high vibration intensities detected during development of the Space Shuttle Main Engine Alternate Turbopump[1]. More recently, water flow[2] and component-level testing of more aggressive inducer designs resulted in varying levels of inducer blade damage. Figure 1 shows the more dramatic consequence of excessive hydrodynamic loads with complete failure of each inducer blade tip. A 1999 investigation[3] into the Japanese H-II-8F launch vehicle failure identified intense cavitation at the turbopump inlet as the most likely cause of inducer blade breakage and subsequent vehicle destruction.

Figure 1. Inducer Blade Damage

Despite these dramatic examples, no description of both the amplitude and frequency content of the cavitation-induced, hydrodynamic loads has been published for any inducer design despite Rosenmann s original investigation[4] into this phenomenon in 1965. As Rosenmann and other investigators[5,6] have confirmed, even and odd number blade inducers often exhibit both stable and rotating cavitation modes depending on the pump operating conditions, whereby cavitation cells may attach themselves to the inducer blades or propagate around the inducer periphery. The pressure imbalance caused by the attached or rotating cavitation cells necessarily develops a force imbalance, which exerts itself on the rotating assembly as a stationary or rotating radial load. The axial location of this radial load moves as the cavitation intensity increases and the inducer flow passages fill with vapor. The cavitation cell number and rotation rate determine the radial load excitation frequency. Whether this excitation force interacts with system structural modes or not depends on the pump operating condition, the system response characteristics, and the relative damping. As such, the experimental devices described here were intended to directly measure these hydrodynamic forces, both in amplitude and frequency content.

ROTATING BALANCE

The following section summarizes the mechanical design, instrumentation, and calibration of the rotating balance. A description of the experimental test article and the data acquisition and reduction process follows.

ROTATING BALANCE MECHANICAL DESIGN

The rotating balance was essentially based on the static wind tunnel balance concept and the approach used to design the flexures was a combination of established methods and more recent experiences with similar design produced for the United States Navy and United Technologies Research Center. The intent was to produce a compact device capable of sensing the hydrodynamically-induced forces generated by an inducer operating in cavitated conditions and resolving the axial and circumferential locations of these forces relative to the inducer. Measurement of six components - normal , side, and axial force and pitch, yaw, and roll moment — were required to locate the integrated load position. The load range requirements summarized in Table 1 then dictated the flexure design and strain gauge requirements. A view of the rotating assembly appears in Figure 2 along with the measured component orientations relative to the inducer and the rotating balance moment reference center location.

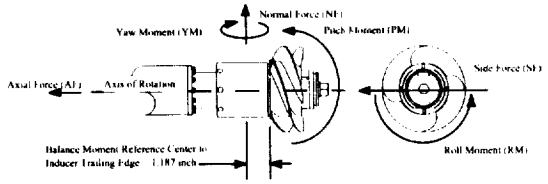

Figure 2. Rotating Assembly with Balance

Table 1. Rotating Balance Components

Component	Load Range
Normal Force (NF)	± 50 pounds-force (± 222 N)
Side Force (SF)	± 50 pounds-force (± 222 N)
Axial Force (AF)	± 500 pounds-force (± 2224 N)
Pitch Moment (PM)	± 300 inch-pounds-force (± 33.9 N-m)
Yaw Moment (YM)	± 300 inch-pounds-force (± 33.9 N-m)
Roll Moment (RM)	± 600 inch-pounds-force (± 67.8 N-m)

ROTATING BALANCE INSTRUMENTATION AND CALIBRATION

The balance flexures were instrumented with semiconductor-type, uni-directional strain gauges arranged in 6 bridges — one for each of the 6 measured components - consisting of from 8 to 16 individual gauges. The instrumented device was waterproofed by the application of a continuous layer of RTV-16. Bridge integrity was verified before and after a water immersion test and after confirmation, the balance was calibrated statically across its intended load range. A calibration fixture and moment arm assembly was used to apply the full range of load combinations, from which the primary and secondary, or interaction, coefficients were calculated. The resulting 6 x 12 calibration matrix in Table 2 was used to convert sensed voltages to engineering units. Estimated measurement error for each component as a percent of full scale also appears in Table 2. The intended goal of 1% full scale or less for each sensed component accuracy was satisfied.

Table 2. Balance Static Calibration Matrix

Interaction Coefficients	Component					
	NF	PM	SF	YM	RM	AF
NF	1.9711E-02	5.6247E-01	-2.9632E-03	-3.6003E-04	6.7089E-03	0.0000E+00
PM	1.2699E-02	5.9365E-02	4.8497E-04	-6.5597E-04	1.6306E-03	4.7540E-03
SF	-3.7769E-03	-2.4474E-03	1.9841E-02	5.6038E-01	-1.5641E-03	0.0000E+00
YM	6.2081E-05	-1.4034E-03	1.1965E-02	6.0062E-02	1.9024E-04	-2.5455E-03
RM	3.1189E-03	-5.8331E-04	-1.2677E-03	1.8419E-03	4.4763E-02	0.0000E+00
AF	8.0683E-04	7.7521E-03	-1.4655E-04	-3.2904E-03	1.1425E-04	8.5287E-02
NF^2	5.6541E-05	3.2500E-05	2.5043E-06	0.0000E+00	-4.1259E-05	0.0000E+00
PM^2	1.0696E-06	-1.2785E-05	0.0000E+00	4.8779E-07	7.1438E-07	7.7018E-06
SF^2	-4.2869E-06	0.0000E+00	-9.7384E-06	-6.0634E-05	0.0000E+00	0.0000E+00
YM^2	-5.9069E-07	-1.5518E-06	6.0694E-07	-1.6958E-05	0.0000E+00	6.6065E-06
RM^2	7.2274E-07	9.3816E-08	1.3467E-08	-1.2136E-07	-2.2892E-06	-3.5818E-07
AF^2	-2.1571E-07	4.1968E-07	-4.7999E-07	7.6642E-06	0.0000E+00	3.7048E-06
Electrical Zero (μV/5V)	-1074	975	-139	215	1479	-277
Percent Full Scale Error (2σ level)	0.58%	0.46%	0.61%	0.34%	0.26%	0.48%

TEST ARTICLE DESCRIPTION

The rotating balance was installed in an existing test article with minor modifications to the existing hardware. As shown in Figure 3, the test article included a full-scale replica of the Space Shuttle Main Engine (SSME) high-pressure liquid oxygen inducer in an axial inlet configuration. The SSME inducer shown in Figure 4 was selected due to its known cavitation performance[7] and the six-vane inlet guide assembly which provided the required inlet velocity profile made the axial inlet arrangement possible. Discharge flow was collected and guided away from the test article in a generic volute with radial exit. The inducer itself includes 4 main blades with moderately swept leading edges. The minor modifications to the existing hardware included separating the inducer inlet fairing from the rotating assembly to reduce the overhung mass. Likewise, the exit diffuser cone was modified to increase the radial clearance around the rotating balance. A small amount of fluid was bled from the main flow and circulated through the balance cavity to stabilize the balance temperature and mitigate and temperature effects on the strain gauges. This leakage flow was extracted downstream of the inducer discharge and returned to the primary flow through the axial clearance just upstream of the inducer leading edge. Two holes in the inducer nut metered this flow and leakage rates of no more than 0.05% of primary flow rate were estimated. A radial clearance of 0.030 inch (0.762 mm) was maintained around the inducer to minimize asymmetry-induced radial loads. A photograph of the uninstrumented balance appears in Figure 5.

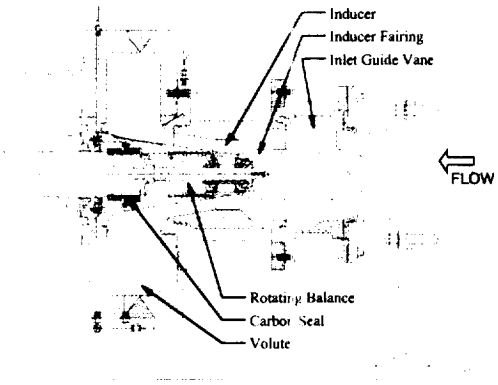

Figure 3. Test Article Cross Section

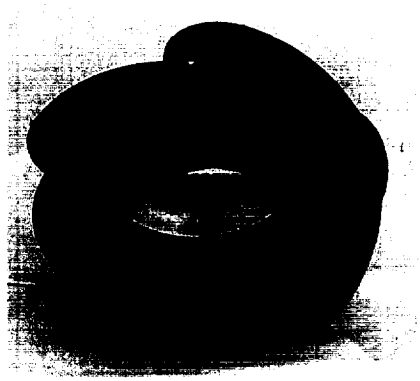

Figure 4. SSME Inducer

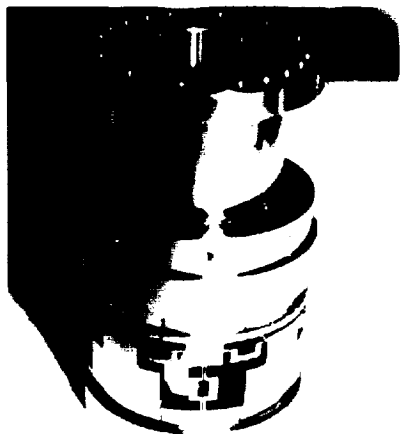

Figure 5. Uninstrumented Rotating Balance

MEASUREMENTS AND DATA ACQUISITION

A combination of steady state and high-frequency response devices were used to measure both inducer and balance performance and to monitor balance health. Steady state pressures were located along the flow path outer diameter both upstream, along the inducer shroud, and downstream of the inducer. Total pressure upstream of the inlet guide vane assembly was measured with a single, shrouded Kiel probe. Likewise, 3 total pressure rakes, with 3 shrouded, total pressure taps each, were installed downstream of the inducer discharge and aligned with the inducer exit flow angle. Flow rate was sensed via a 6-inch turbine-type flow meter while shaft speed was sensed through a magnetic collar and pickup device. High-frequency-response pressure transducers were located upstream of the inducer, at the leading edge, the inducer mid-chord, and slightly downstream of the inducer for complete mapping of the unsteady environment. At the inducer leading edge and downstream location, 3 transducers were included for cavitation cell train phase identification. These measurement locations are summarized in

Table 3. In addition, bearing outer race, slip ring, and water temperatures were recorded

Table 3. Measurement Details

Location	Static Pressure	Total Pressure	Unsteady Pressure
Upstream of IGV	2	1	1
Upstream of Inducer	3	0	0
Inducer Leading Edge	3	0	3
17% Chord	1	0	0
30% Chord	1	0	0
50% Chord	1	0	3
67% Chord	1	0	0
83% Chord	1	0	0
Inducer Trailing Edge	3	0	0
Downstream of Inducer	3	9	3

The data acquisition system used to collect the rotating balance data appears schematically in Figure 6. Two semi-parallel systems were employed; one consisting of a LabView-based analog-to-digital converter with relatively limited bandwidth, the second a true high-frequency, 32-channel data system with bandwidth of 10,000 Hertz. A common power supply provided the required 5 volts to the balance bridges. The LabView-based system continuously sampled balance voltages, held these values in a buffer, and displayed or stored averaged values of voltage and processed engineering units. This system provided averaged or DC values and also served as a health monitor. The high-frequency data acquisition system recorded both balance voltages as well as test article operating conditions, unsteady shroud pressures, and accelerations. A second LabView-based system was used to collect and process the steady state measurements such as pressures, temperatures, flow rate, speed, and differential pressures. Steady state data was sampled from 100 to 1000 times and the population mean and standard deviation stored in engineering units.

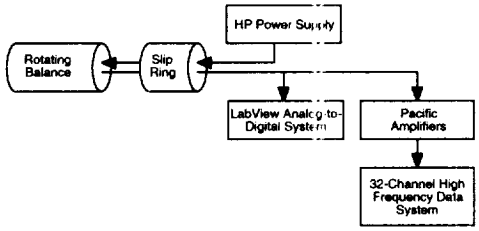

Figure 6. Balance Data Acquisition Schematic

EXPERIMENTAL TEST PLAN

The experimental test included three series: 1) modal test, 2) air spin test, and 3) water test. The incremental approach allowed for the rotating balance performance to be monitored under increasingly harsh operating conditions, thereby building confidence while minimizing risk to the device. The modal test was conducted to measure the balance s structural response at various excitation frequencies. This data would later be used to define the upper limit of the device s measurement bandwidth. Likewise, the air spin test was conducted to directly measure the rotating assembly's unbalance up to a maximum operating speed of 5000 revolutions per minute. This data would be subtracted from the measured data in water to remove the built-in static load. The final test series included operating at scaled conditions in water from 80% to 120% of the design flow coefficient. The original test plan included water testing from non-cavitated condition to complete head breakdown. Unfortunately, rotating balance load limits prevented testing at the highest suction specific speed. Table 4 summarizes the test series details and operating conditions.

Table 4. Experimental Test Series

Series	Percent Design Flow Coefficient	Suction Specific Speed	Speed (rpm)	Comments
Modal Test	N/A	N/A	0	Carbon Seal Removed
Air Spin	N/A	N/A	300 — 5000	Carbon Seal Removed
Water Test 1	90% - 110%	5000 — Balance Load Limit	2200, 3200, 3800	High Frequency Data Only
Water Test 2	80% - 120%	5000 — Balance Load Limit	2200, 3200, 3800	Steady Performance Data Only

Design Flow Coefficient = 0.161

ROTATING BALANCE DATA REDUCTION

Sensed voltages were converted to engineering units by first subtracting the measured electrical zero from each component and then processing the resulting voltages through the calibration matrix. The method from Smith[8] was used, whereby the calibration matrix was converted to three matrices representing the primary sensitivities and the first and second order interaction coefficients. Data across the entire measured bandwidth was processed in this fashion by the high-frequency data system. The parallel LabView system — used primarily for health monitoring — followed a similar, iterative approach using time averaged values as inputs. The LabView system averaged sensed voltages over a 0.25 second interval, subtracted the electrical zero from the static calibration, and iteratively solved for the 6 components or force and moment. Since all the raw voltages were also recorded and stored, these measurements were later reprocessed by first subtracting the measured electrical zeros from the raw values and the loads recomputed.

SURFACE MOUNT PRESSURE TRANSDUCERS

A description of the transducers themselves and the experimental verification test follows.

TEST ARTICLE DESCRIPTION

The experimental test article shown in Figure 7 included 2 Kulite-brand, miniature pressure transducers mounted directly on the surface of an exposed disk. The disk itself was installed in the water test facility via a stainless steel tee, modified slightly to get the pressure transducers as close to the passing flow stream as possible. A photograph of the installed test article appears in Figure 8. The reference devices were Kistler-brand, high-frequency response pressure transducers, type 211b.

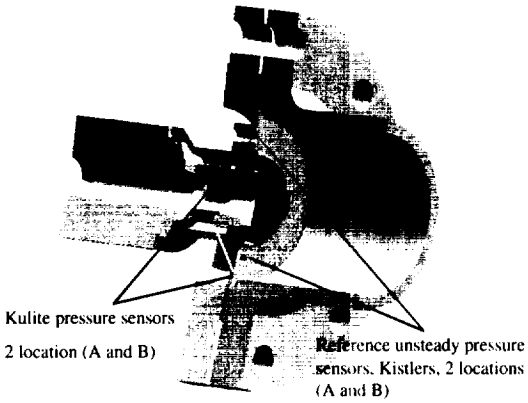

Figure 7. Experimental Test Article

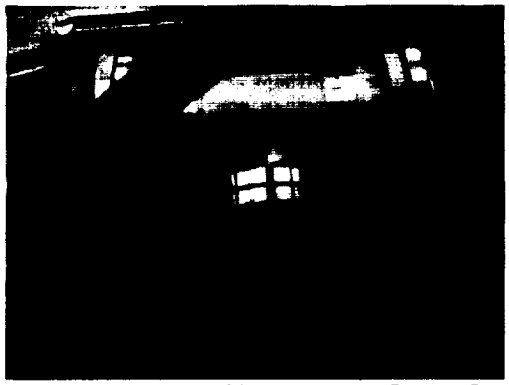

Figure 8. Photograph of Test Article in Facility Piping

EXPERIMENTAL TEST PLAN

In order to evaluate both performance and integrity in water, the devices were installed in the test article and the test article installed in the facility piping immediately downstream of a gate valve. After a period of immersion to insure against water contamination, water was circulated through the facility piping with the upstream gate valve used as a noise generator. Various flow rates and mean pressures were set and both Kulite and Kistler outputs recorded using the same high-frequency data acquisition system described previously.

RESULTS

Experimental results from both the rotating balance evaluation and surface-mount pressure transducer test follow.

ROTATING BALANCE UNLOADED ZEROES

A series of static loads were applied to the balance only for an end-to-end verification of the measurement system and control software. These checks[9] revealed a significant hysteresis effect on all measured components with axial force most affected. Residual loads as high as two percent of the component full scale were observed. This effect was attributed to the waterproofing method whereby virtually the entire circumference of the rotating balance at the flexure location was coated with RTV-167. The waterproofing was found attached to both the metric and non-metric ends of the flexure areas, and, combined with the observed hysteresis, suggested that some portion of the load was being absorbed by the waterproofing material. Likewise, the unloaded zero values for each component continued to drift throughout the experimental test, although the normal and axial force components exhibited the largest variations. The measured component zero values as percent of full-scale load are plotted in Figure 9 versus test date for the water test series. These values were averages computed from two continuous hand revolutions. The sensed zeros for the air spin series remained within 1% of the calibration electrical zero values in Table 2. To mitigate these effects, the rotating balance zeroes were measured immediately before and after each test run and these values were then applied in the data reduction process.

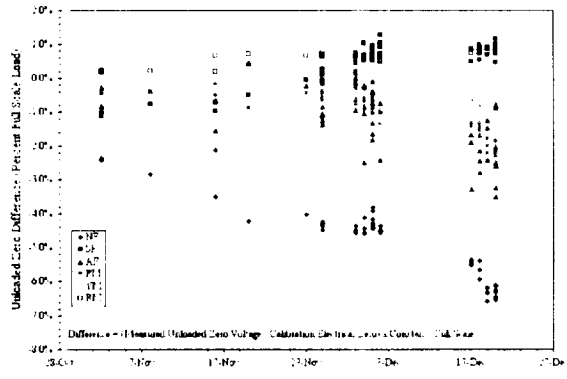

Figure 9. Balance Zero Drift in Water

MODAL TEST RESULTS

A modal test was conducted in June of 2001 following test article installation into the test facility.

The test was conducted in-situ to insure that all relevant structural contributions would be accurately captured since the modal test output — structural amplification versus excitation frequency — would be used to limit or correct all rotating balance measurements. Figure 10 shows the experimental results with structural amplification factor versus frequency for each sensed load component. As predicted by the rotordynamics model, the first measured structural mode appeared at 217 Hertz. However, the actual bandwidth was essentially limited to approximately 34 Hertz after selecting a maximum structural magnification factor of 5%. This limit also appears on Figure 10.

Normalizing these frequencies by the maximum shaft speed results in values of 3.43 for the structural mode and 0.53 at the 5% structural magnification limit. The lower value limits the rotating balance measurement bandwidth to essentially DC response, as any hydrodynamic excitation sources at higher frequencies would be amplified structurally. As such, only the DC or synchronous averaged values for sensed forces and moments will be presented here.

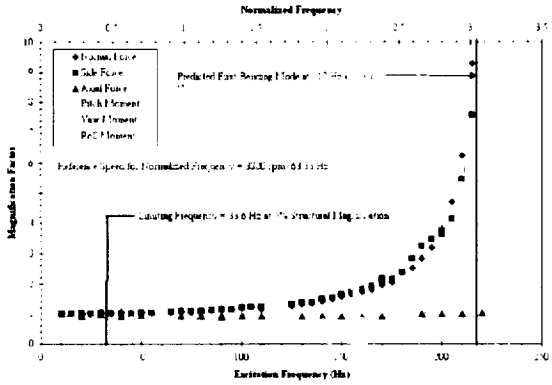

Figure 10. Structural Magnification versus Frequency

AIR SPIN RESULTS

The air spin tests were conducted both to verify the balance sensitivity and to directly measure the built-in unbalance. A total unbalance of 0.058 ounce-inches (0.042 g-m) at an angle of 8.43 degrees relative to the balance was measured. This unbalance was not subtracted from the results presented here.

WATER FLOW TEST RESULTS

Sufficient measurements were incorporated into the test article to verify inducer steady state performance both to insure hydrodynamic performance matched that from previous experimental tests of the same inducer and to compute inducer efficiency. The inducer suction performance appears in Figure 11 versus percent design flow coefficient along with experimental data at the design flow coefficient from a previous water flow test[10]. The reductions in steady head rise at 90% and 100% of the design flow coefficient were previously observed to correspond with the transition from a steady, four-blade cavitation mode to an alternate blade cavitation mode. The measured composite, 2 x synchronous, and 4 x synchronous-averaged unsteady pressures at the inducer inlet at the design flow coefficient at 3800 revolutions per minute are plotted in Figure 12 versus suction specific speed. The high-frequency response devices provide a more accurate indication of cavitation mode and illustrate the contribution of these harmonics to the total fluctuating pressure intensity.

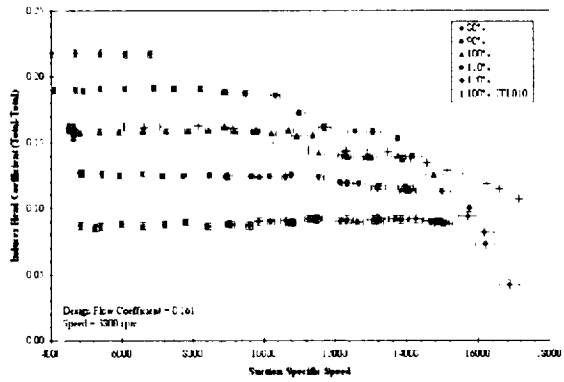

Figure 11. Inducer Head Coefficient versus Suction Specific Speed at 3800 rpm

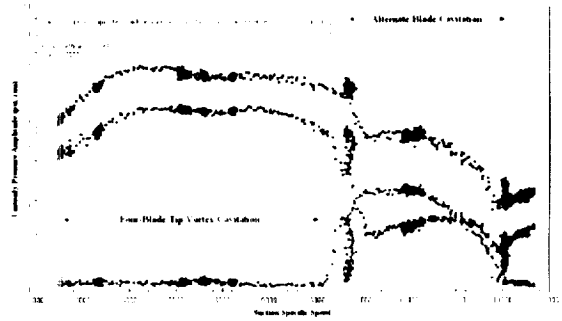

Figure 12. Shroud Unsteady Pressure at Inducer Inlet versus Suction Specific Speed at Design Flow Coefficient and 3800 rpm

Head coefficient versus percent design flow coefficient in Figure 13 was collected at and below a suction specific speed of 6000. This regime is labeled as non-cavitated due to its level head rise versus suction specific speed characteristics despite the relatively small, vortex-type cavitation previously observed (insert reference here) attached to each of the four inducer blades. Both total-to-total and static-to-static head rise are included in Figure 13 with the upstream value for each measured upstream of the inlet guide vane assembly.

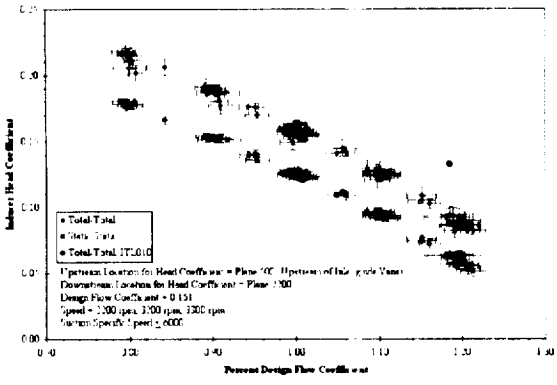

Figure 13. Inducer Head Coefficient versus Percent Design Flow Coefficient

Since the rotating balance measurements were severely restricted to avoid structural magnification, only the DC or synchronous averaged values for the sensed forces and moments were considered valid. Although this restriction eliminated all the higher-frequency-content data, the synchronous averaged loads confirmed that the device could accurately sense the magnitude and relative orientation of the integrated hydrodynamic forces. Figure 14 shows the progression from the four-blade cavitation mode to an alternate blade cavitation mode at the design flow coefficient and constant speed and the corresponding adjustment in radial load magnitude and direction. As the four-blade cavitation intensity increases, the load magnitude also increases until the cavitation mode adjusts to the alternate blade cavitation mode. A corresponding reduction in radial load was observed at this transition along with an adjustment in the orientation of the load relative to the inducer.

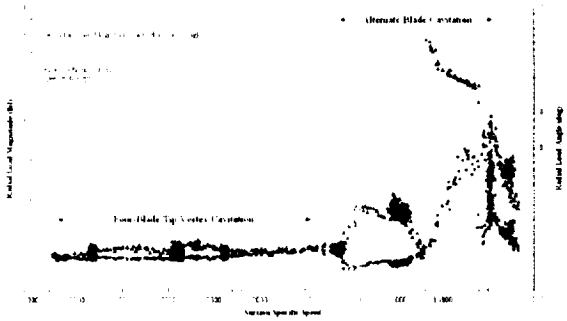

Figure 14. Steady Radial Load Magnitude and Angle versus Suction Specific Speed at Design flow Coefficient and 3800 rpm

However, the synchronous-averaged axial force and roll moment were valid indicators of inducer performance, since roll moment was essentially shaft torque. Inducer hydraulic efficiency and thrust, normalized by the square of speed, appear in Figure 15. Unlike the previous results, the unbalance and air tare has been included in the calculations.

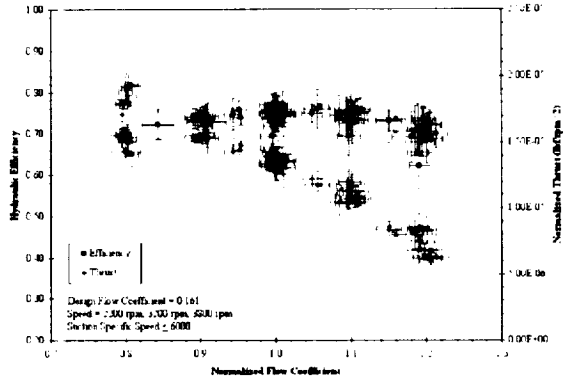

Figure 15. Hydraulic Efficiency and Normalized Thrust versus Percent Design Flow Coefficient

For comparison, Figures 16 and 17 include spectrograms of the sensed fluctuating pressure and normal force magnitudes up to 500 Hertz at the design flow coefficient at 3800 revolutions per minute. The cavitation modes in Figure 17 are indicated along with the corresponding frequencies in the rotating reference frame. Although the rotating balance data was considered invalid above approximately 34 Hertz, Figure 17 provides a qualitative insight into the frequency content of the hydrodynamic loads in the rotating reference frame.

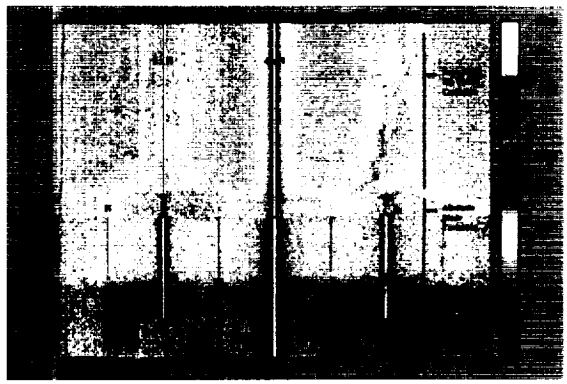

Figure 16. Unsteady Pressure Spectrogram at Inducer Mid-Chord Location at Design Flow Coefficient and 3800 rpm

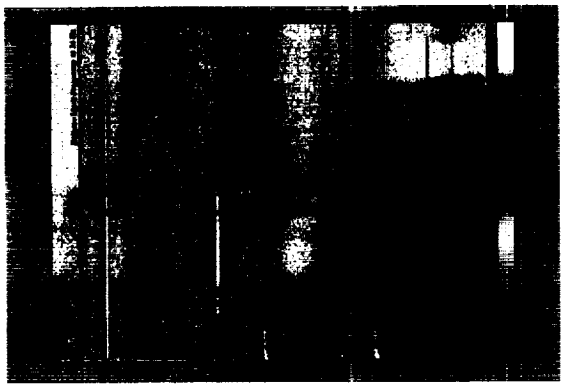

Figure 17. Normal Force Spectrogram at Design Flow Coefficient and 3800 rpm

MINIATURE PRESSURE TRANSDUCER STATIC PERFORMANCE

A small temperature-induced bias offset was observed for both surface-mount transducers of approximately 2% of the full-scale range during static pressure excursions. This was comparable to manufacturer s specifications.

MINIATURE PRESSURE TRANSDUCER DYNAMIC PERFORMANCE

Figures 18 through 21 summarize the surface-mount transducers dynamic performance in terms of gain and phase relative to the reference devices. Only spectral content with greater than 90% coherence included. Gains from 0.99 to 1.08 were computed along with small phase differences from —6.80 to 3.40 degrees.

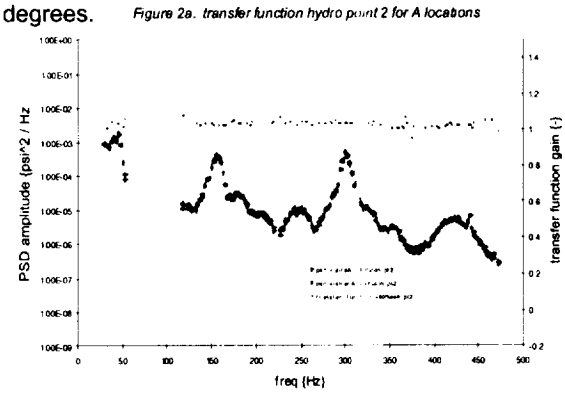

Figure 18. Transfer Function, Kulite A to Kistler A

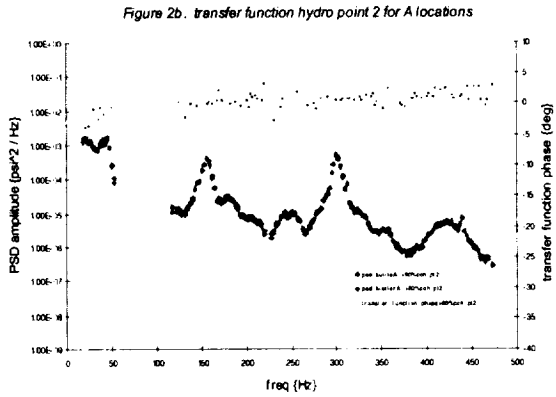

Figure 19. Phase versus Frequency, Kulite A to Kistler A

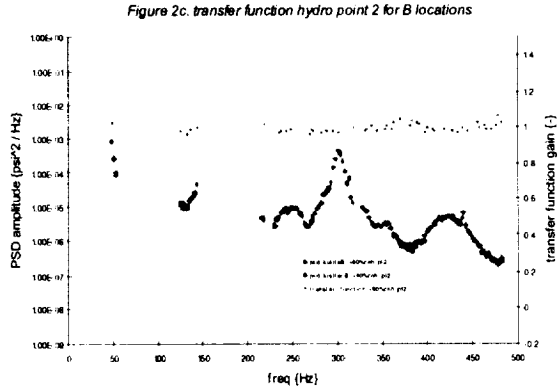

Figure 20. Transfer Function, Kulite B to Kistler B

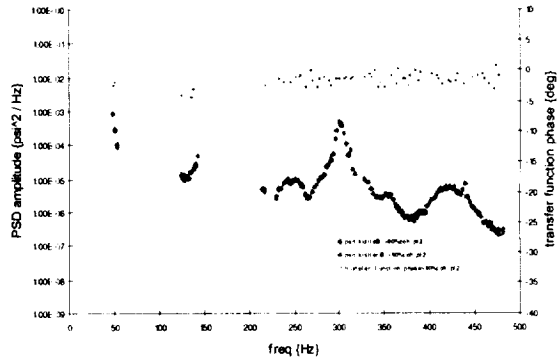

Figure 21. Phase versus Frequency, Kulite B to Kistler B

UNCERTAINTY ANALYSIS

An uncertainty analysis incorporating the experimental precision and bias errors using the root-sum-square method of Coleman and Steele[11] was performed to estimate the uncertainties associated with the measured and calculated quantities. A 95% confidence level was assumed. The estimated uncertainties for each of the parameters presented

here are summarized in Table 5 and represent the maximum computed uncertainty value for all test points.

Table 5. Calculated Uncertainties

Parameter	Uncertainty
Flow Coefficient	0.004
Inducer Head Coefficient (T-T)	0.007
Inducer Head Coefficient (S-S)	0.006
Suction Specific Speed	380 rpm-gpm^2/ft$^{3/4}$
Radial Load	0.42 pounds-force (1.86 N)
Moment	1.72 inch-pounds-force (0.194 N-m)
Axial Force	2.41 pounds-force (10.7 N)
Roll Moment	1.65 inch-pounds-force (0.186 N-m)
Hydraulic Efficiency	0.062
Normalized Thrust	1.030e-06 rpm/lbf^2 (5.206e-08 rpm/N^2)
Unbalance	0.016 ounce-inch (0.042 gm-m)

SUMMARY AND CONCLUSIONS

Although this document was intended to summarize the preliminary results of these experimental validation tests, a few general conclusions regarding the cavitation sensors can be made:

1. Rotating balance bandwidth was severely restricted by the relative softness of the device itself to approximately 34 Hertz.
2. Integrated radial load and orientation of the load relative to the balance was sensitive both to cavitation mode and cavitation intensity.
3. Surface-mount pressure transducers accurately tracked static pressure with only small temperature-induced bias shift.
4. Surface-mount pressure transducer dynamic response matched that of the reference devices.

Follow-up work will address the bandwidth limitation by pursuing an advanced balance design with both increased load capacity and increased structural rigidity. The next phase of surface-mount pressure transducer evaluations will include testing the devices in a rotating, cavitating environment.

ACKNOWLEDGEMENTS

Wayne Bordelon, who provided valuable guidance and assistance during the experimental test, first proposed the balance concept. Personnel from the Experimental Fluid Dynamics Group at MSFC assisted with the experimental test and special recognition goes to Doug McBride and Bo Jones for their valuable insight and electrical and mechanical skills.

REFERENCES

[1] Ryan, R.S., Gross, L.A., Mills, D., and Mitchell, P., The Space Shuttle Main Engine Liquid Oxygen Pump High-Synchronous Vibration Issue: The Problem, The Resolution Approach, The Solution, AIAA 94-3153, June, 1994.

[2] Skelley, S.E., Fastrac Liquid Oxygen Turbopump Water Flow Post Test Report, MSFC memorandum TD63-99-023, November, 1999.

[3] NASDA Office of Space Transportation Systems, Launch Failure of H-II-8F Launch Vehicle: Cause of Failure Investigated through Various Analyses, June, 2000.

[4] Rosenmann, W., Experimental Investigation of Hydrodynamically Induced Shaft Forces with a Three-Bladed Inducer, Symposium on Cavitation in Fluid Machinery, ASME Winter Annual Meeting, November, 1965.

[5] Acosta, A.J., An Experimental Study of Cavitating Inducers, Second Symposium on Naval Hydrodynamics, Office of Naval Research, August, 1958.

[6] Kamijo, K., Yoshida, M., and Tsujimoto, Y., Hydraulic and Mechanical Performance of LE-7 Lox Pump Inducer, *Journal of Propulsion and Power*, Vol. 9, No. 6, 1993.

[7] Bordelon, W.J., Gaddis, S.W., and Nesman, T.E., Cavitation Environment of the Alternate High Pressure Oxygen Turbopump Inducer, Cavitation and Multiphase Flow Forum, ASME FED Vol. 210, 1995.

[8] Norman, R., Rotating Balance Static Check Load Data Report, MSFC memorandum TD74-01-01, April, 2001.

[9] Coleman, H.W. and Steele, W.G., Experimentation and Uncertainty Analysis for Engineers, John Wiley and Sons, New York, 1989.

[10] Gaddis, S.W., Alternate Turbopump Development High Pressure Oxidizer Turbopump Second Source Inducer Water Flow Rig Test Plan, MSFC memorandum ED34-97-024, May, 1997.

[11] Coleman, H.W. and Steele, W.G., Experimentation and Uncertainty Analysis for Engineers, John Wiley and Sons, New York, 1989.

MAR 22 R

National Aeronautics and Space Administration

NASA Scientific and Technical Document Availability Authorization (DAA)

Use this form for all STI that is to be released outside of NASA. See Instructions on page 3.

☒ ORIGINAL ☐ MODIFIED

I. DOCUMENT/PROJECT IDENTIFICATION

TITLE	AUTHOR(S)
Inducer Hydrodynamic Load Measurement Devices	Stephen E. Skelley Thomas F. Zoladz
ORIGINATING NASA ORGANIZATION *(Include organization code)* MSFC/Technology Transfer Department/CD30	PERFORMING ORGANIZATION *(If different)* MSFC/Fluid Physics and Dynamics Group/TD63
CONTRACT/GRANT/INTERAGENCY/PROJECT NUMBER(S)	DOCUMENT NUMBER(S) / DOCUMENT DATE

CHECK: ☒ Conference ☐ Periodical ☐ Journal Name ☐ Book Title ☐ Publisher ☐ URL
and enter name, place, and date to right, if applicable.
Route through center or HQ Export Control Administrator. ▶

2002 JANNAF Subcommittee Joint Meeting
Destin, FL
April 8-12, 2002

II. NATIONAL SECURITY CLASSIFICATION *(Check one of the four boxes)*

☐ TOP SECRET ☐ SECRET ☐ CONFIDENTIAL ☒ UNCLASSIFIED

III. AVAILABILITY CATEGORY

(Author indicates ITAR or EAR, if appropriate. Author indicates USML or ECCN/CCL numbers, if known. Center or HQ Export Control Administrator must concur in Section VIII)

NASA EXPORT-CONTROLLED PROGRAM STI

☐ International Traffic in Arms Regulations (ITAR)

☐ Export Administration Regulations (EAR)

Export-Controlled Document - U.S. Munitions List (USML Category) _____ or
Export Control Classification Number (ECCN) _ from the
Commerce Control List (CCL) _____

CONFIDENTIAL COMMERCIAL STI *(Check appropriate box below and indicate the distribution limitation (see Additional Information and "Limited until (date)" if applicable):*

☐ TRADE SECRET
☐ Small Business Innovation Research (SBIR)
☐ COPYRIGHTED *(indicate appropriate distribution limitation (see Additional Information), if applicable).*

☐ Limited until *(date)*- if applicable _____
☐ Limited until *(date)*- if applicable _____
☐ Limited until *(date)*- if applicable _____
☐ Publicly available *(but subject to copying restrictions)*

ADDITIONAL INFORMATION *(Check appropriate distribution limitation below and/or limited until (date) above, if applicable).*

☐ U.S. Government agencies and U.S. Government agency contractors only
☐ U.S. Government agencies only
☐ NASA personnel & NASA contractors only
☐ NASA contractors and U.S. Government only
☐ NASA personnel only
☐ Available only with approval of issuing office: _____

☒ Publicly Available STI

Publicly available means it is unlimited and unclassified, is not export-controlled, does not contain confidential commercial data, and has cleared any applicable patent application.

NASA FORM 1676 AUG 01 PREVIOUS EDITION IS OBSOLETE.

IV. DOCUMENT DISCLOSING AN INVENTION

☐ If STI discloses an invention, Author/Originator must check box and send to Patent Counsel.

THIS DOCUMENT MAY BE RELEASED ON (date) _____

NASA HQ OR CENTER PATENT OR INTELLECTUAL PROPERTY COUNSEL SIGNATURE:

DATE:

V. BLANKET AVAILABILITY AUTHORIZATION *(OPTIONAL)*

☐ This blanket availability authorization is granted on *(date)* _____
All documents issued under the following contract/grant/project number may be processed as checked in Sections II and III

CHECK ONE: ☐ Contract ☐ Grant ☐ Project Number _____

SIGNATURE _____

MAIL CODE _____

The blanket availability authorization granted on *(date)* _____ is

☐ RESCINDED - Future documents must have individual availability authorizations.

☐ MODIFIED - Limitations for all documents processed in the STI system under the blanket release should be changed to conform to blocks as checked in Sections II and III.

SIGNATURE _____

MAIL CODE _____ DATE _____

VI. AUTHOR/ORIGINATOR VERIFICATION

I HAVE DETERMINED THAT THIS PUBLICATION:

☐ DOES contain ITAR/export-controlled, confidential commercial information, and/or discloses an invention and the appropriate limitation is checked in Sections III and/or IV.

☒ Does NOT contain ITAR/export-controlled, confidential commercial information, nor does it disclose an invention and may be released as indicated above.

SIGNATURE Stephen Scott DATE 3/14/02

VII. PROJECT OFFICER/TECHNICAL MONITOR/DIVISION CHIEF REVIEW OF I THRU VI

☒ APPROVED FOR DISTRIBUTION AS MARKED ☐ NOT APPROVED

NAME	MAIL CODE	SIGNATURE	DATE
Jim Turner	TD60	for Preston Jones	3/22/02

VIII. EXPORT CONTROL REVIEW/CONFIRMATION

☒ Public release is approved

☐ Export-controlled limitation is approved

☐ Export-controlled limitation is not applicable

☐ Export-controlled limitation (ITAR/EAR marked in Section III is assigned to this document)

USML CATEGORY NUMBER	CCL NUMBER, ECCN NUMBER	CENTER OR HQ EXPORT CONTROL ADMINISTRATOR SIGNATURE	DATE
		H. J. Dennis, Jr.	3-19-02

IX. DAA FINAL APPROVAL

☐ APPROVED FOR DISTRIBUTION AS MARKED IF REQUIRED BY YOUR CENTER

☐ NOT APPROVED

SIGNATURE Blanket authorization-NASA HQs letter of

MAIL CODE R DATE 3/23/94

Joyce E. Turner
NASA-Marshall Spc Flt Ctr
MSFC, AL 35812

X. DISPOSITION

SEND THIS FORM, WHEN COMPLETED, TO YOUR CENTER'S RESPONSIBLE OFFICE OR TECHNICAL PUBLICATIONS OFFICE.

CD70/Edward D. Medal 3/27/02

AD38/Joyce E. Turner Waits 03-28-02

544-4628

NASA FORM 1676 AUG 01 PREVIOUS EDITION IS OBSOLETE.